Light diffusion and localization in three-dimensional nonlinear disordered media

C. Conti,[1,2] L. Angelani,[3] and G. Ruocco[2,4]
[1]*Centro Studi e Ricerche "Enrico Fermi," Via Panisperna 89/A, I-00184, Roma, Italy*
[2]*Research Center Soft INFM-CNR, c/o Università di Roma "La Sapienza," I-00185, Roma, Italy*
[3]*Research Center SMC INFM-CNR, c/o Università di Roma "La Sapienza," I-00185, Roma, Italy*
[4]*Dipartimento di Fisica, Università di Roma "La Sapienza," I-00185, Roma, Italy*
(Received 21 July 2006; published 26 March 2007)

By using a three-dimensional finite-difference time-domain parallel code, the linear and nonlinear propagation of light pulses in a disordered assembly of scatterers, generated by a molecular dynamics code, is simulated. We calculate the static and dynamical light diffusion constant and the transmission in the presence of localized states. We numerically demonstrate the "modulational instability random laser": at high input peak power, energy is transferred to localized states from the input pulse, resulting in a power-dependent nonexponential time decay of the transmitted pulse.

DOI: 10.1103/PhysRevA.75.033812 PACS number(s): 42.25.Dd, 42.55.Zz, 82.70.Dd, 42.65.−k

I. INTRODUCTION

Electromagnetic wave localization and diffusion in random media have been recently considered by several authors. Experimental studies reported on various evidences of light localization, including the existence of a nonexponential long-time tail of the transmitted intensity [1–5], and these processes were considered in numerous theoretical and numerical papers (as, e.g., in Refs. [6–11]). In a purely diffusive regime, pulsed light impinging on a disordered sample is rapidly dispersed while propagating; this implies that nonlinear effects are typically negligible. This holds true as far as localization processes do not get involved. For example, in random lasers (for a recent review see Ref. [12]), localized or extended modes [13] are excited in a disordered medium by means of an optically active material; in this case, the large resonant nonlinear susceptibility and the fact that long living (high Q) modes are excited foster a variety of nonlinear phenomena (as, e.g., in Refs. [14–16]). For nonresonant ultrafast nonlinearities (as $\chi^{(3)}$ processes of electronic origin), it is in principle possible to use high-peak intensity femtosecond laser pulses to induce nonlinear effects, even in the presence of strong light diffusion. However, the (numerical and theoretical) analysis is enormously complicated by the need to include various effects as disorder, nonlinearity, material dispersion and to take into account a three-dimensional (3D) environment. Even in the absence of nonlinearity, no "*ab initio*" numerical investigation of 3D Maxwell equations for femtosecond pulses in disordered media has been reported, to the best of our knowledge. Some theoretical investigations considered the role of the Kerr effect (i.e., an intensity dependent refractive index) for a monochromatic excitation [17,18]; however, ultrafast $\chi^{(3)}$ optical nonlinearity may also provide other mechanisms. We specifically consider the gain of nonresonant origin, i.e., the optical parametric oscillation (OPO). OPO, in isotropic media in the absence of disorder, has been recently considered with reference to various devices [19–21], while in the fiber-optics community it is known as the "modulational instability laser" [22]. Here we report on the extensive $3D+1$ numerical analysis of linear diffusion and nonlinear amplification processes in a random dispersive nonlinear medium. We use a molecular dynamics (MD) code for generating a three-dimensional distribution of spherical scatterers and a finite-difference time-domain (FDTD) parallel algorithm for simulating light propagation. The MD-FDTD approach not only reproduces the diffusive regime in agreement with reported experimental results in the linear regime, but also provides clear indications of the random OPO process, with analogies to random lasers.

II. THE MOLECULAR-DYNAMICS-DRIVEN FDTD

An "*ab initio*" investigation of the nonlinear light propagation in 3D disordered media, requires a realistic distribution of a colloidal medium and of its nonlinear dielectric response. We model the disordered system as an assembly of polydispersed particles in air. The MD code generates the particle configuration; specifically, we considered a 50:50 mixture of spheres with diameter ratio 1.2, interacting by a 100–200 Lennard Jones potential [23]. The considered sample is composed by 1000 scatterers; once determined the particle positions by the MD code, each of them is taken as filled by a dispersive optically nonlinear medium, which is modeled as described below. The particle dimensions are chosen in order to simulate typical samples used in light localization and diffusion experiments, as, e.g., in Refs. [1,24]. We considered diameters for the biggest particles in the mixture ranging from 200 nm to 400 nm; correspondingly the volume filling fraction ϕ for our samples, with volume L^3 ($L=4$ μm, of the order of the values considered in [3]), varies in the interval $\phi \in [0.1, 0.6]$. The optical linear response of the particle medium is chosen as the best approximation of that of TiO_2, used in most of the reported experiments, including material dispersion. The latter is modeled by a single-pole Lorentz medium, reproducing the data for TiO_2 reported in Ref. [25]. Material absorption is also included providing an absorption coefficient $\kappa_i = 10$ mm^{-1} at $\lambda = 514$ nm. The 3D Maxwell equations, solved by the parallel FDTD [26] algorithm, are written as

$$\nabla \times \mathbf{E} = -\mu_0 \partial_t \mathbf{H}, \quad \nabla \times \mathbf{H} = \epsilon_0 \epsilon_\infty \partial_t \mathbf{E} + \partial_t \mathbf{P},$$

$$\partial_t^2 \mathbf{P} + 2\gamma_0 \partial_t \mathbf{P} + \omega_0^2 f(P)\mathbf{P} = \epsilon_0(\epsilon_s - \epsilon_\infty)\omega_0^2 \mathbf{E} \quad (1)$$

The nonresonant nonlinear response is determined by the nonlinear Lorentz oscillator. As $f(P)=1$, Eqs. (1) model the linear dispersive medium TiO_2; by appropriately choosing $f(P)$, the system displays an isotropic ultrafast nonlinearity, as previously described in Ref. [19], including the nonresonant $\chi^{(3)}$ susceptibility. In the present case, the associated Kerr effect has a nonlinear refractive index $\Delta n = n_2 I$, with I the optical intensity and $n_2 \cong 10^{-18}$ m^2 W^{-1}. The parameters in TiO_2 particles are given by (MKS units): $\epsilon_s = 5.9130$, $\epsilon_\infty = 2.8731$, $\omega_0 = 6.6473 \times 10^{15}$, $\gamma_0 = 8.9168 \times 10^{11}$, and $f(P) = [1 + (P/P_0)^2]^{3/2}$ with $P_0^{-2} = 3.0$; out of the particles, $P=0$ and $\epsilon_s = \epsilon_\infty = 1$ (vacuum).

The code is parallelized using the "MPI" protocol, and "UPML" absorbing boundary condition are used in the three spatial directions [26]. The used discretization is $\Delta x = \Delta y = \Delta z \cong 30$ nm and $\Delta t \cong 0.02$ fs. The z-propagating input beam is taken with a Gaussian TEM_{00} linearly y-polarized profile, at the input face of the disordered medium its waist is $w_0 = 1$ μm. The input pulse temporal profile is Gaussian, with duration $t_0 = 100$ fs and carrier wavelength $\lambda = 520$ nm. The numerical results have been verified a number of times by halving the spatiotemporal discretization. The validity of our approach has been confirmed in a variety of studies, as, e.g., in Refs. [19,27].

III. ONSET OF LIGHT DIFFUSION

The first numerical simulations were aimed to investigate light diffusion when the nonlinear effects can be taken as negligible (low power), for a fixed sample spatial extension. We considered increasing values for the diameter of the spheres in the mixture; in the following σ is the corresponding value of the biggest particles in the considered 50:50 mixture (for the others, the diameter is $\sigma/1.2$). This corresponds to increase the average density of the medium, as well as the volume packing fraction. In order to unveil the onset of diffusion, we monitored the time-dependent output intensity, which is expected to develop an exponential tail in the diffusive regime. This is obtained in two ways: (i) we considered the electric field E_y at one point in the middle of the output face of the sample (see Fig. 1), and we calculated the "local intensity" by squaring the field and filtering with a low pass filter to remove the optical carrier (thus mimicking a photodiode); (ii) we considered the total transmission from the output face of the sample as the calculated z component of the Poynting vector, integrated with respect to the transverse x, y coordinates.

In Fig. 1 we show the results for the local intensity, while increasing the volume filling fraction ϕ. In order to compare the trailing edge of the transmitted pulses, for each signal we rescaled the peak value to the unity and shifted the temporal axis to make all the peaks for any σ coincident. At high packing fraction the onset of an exponential trend is clearly visible. Note the residual oscillations, that are due to the fact that light is collected in a specific point at the output face. A typical far-field speckle pattern calculated from our simulation is shown in the inset of the bottom panel, and obtained

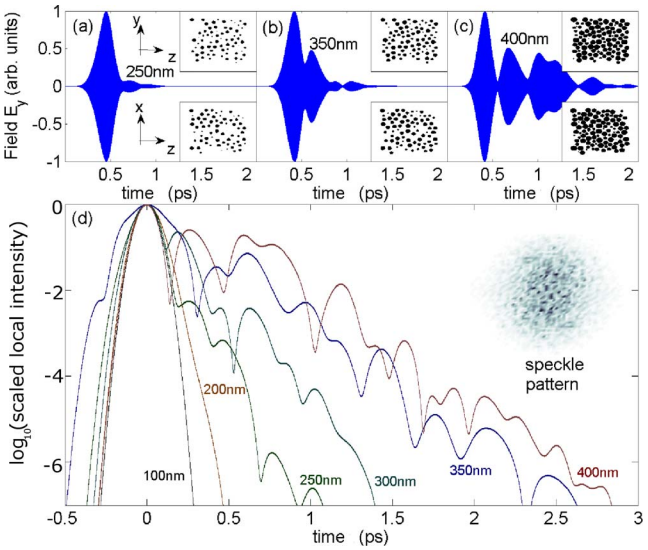

FIG. 1. (Color online) Top panels (a)–(c): electric field in the middle of the output face of the sample at low input peak power ($P_{in} = 1$ nW), for three different particle diameters ($\sigma = 250, 350, 400$ nm). The insets show the particle distribution in the yz (top) and xz (bottom) middle section of the sample. Bottom panel (d): normalized local intensity in logarithmic scale (the peak intensity is scaled to unity). The inset shows the calculated speckle pattern.

by storing the E_y component of the electric field in the output section, Fourier transforming with respect to the transverse coordinates, and averaging over time (the pattern is calculated for a continuous wave excitation at $\lambda = 520$ nm).

The intensity modulation in Fig. 1 disappears when considering the overall transmission from the output facet, which provides an average information over all the speckles and is shown in Fig. 2. The instantaneous flux for the z component of the Poynting vector is calculated and then filtered to remove the reactive component. The appearance of an exponential tail in the transmission denotes the transition to the diffusive regime. Note that the exponential trend is maintained up to the maximum time considered $t \cong 7$ ps (corresponding to transmission levels around 10^{-15}), but we limited the figure to $t \cong 3$ ps for the sake of clearness.

The transmitted signal is $I(t) \propto \exp[-\pi^2 D(t) t / L^2]$, with an instantaneous diffusion coefficient $D(t) \to D$ as $t \to \infty$ and a sample length L. When the packing fraction increases, the tail gets longer due to the reduced diffusivity D. The latter quantity is shown in Fig. 2(b) vs ϕ. The results are in agreement with experimentally determined values, as reported in literature (e.g., in Refs. [1,3,24]). Note that, as expected, D decreases as the volume packing fraction increases, and at high ϕ the diffusivity tends to an asymptotic value (for non overlapping particles). The inset in Fig. 2(b) shows the calculated instantaneous diffusivity for two values of σ, which reproduces the reported trends, including some temporal oscillations [1,28].

IV. LIGHT DIFFUSION IN PRESENCE OF NONLINEARITY

Next, we consider the diffusive regime for a fixed $\sigma = 400$ nm ($\phi \cong 0.6$), while increasing the input peak power

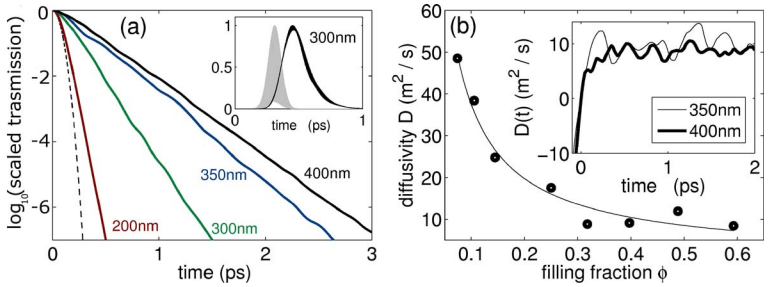

FIG. 2. (Color online) (a) Tail of the normalized transmitted pulse (the flux of the z component of the Poynting vector at the output face) for various particle diameters; the normalization is such that the transmission peak is scaled to unity. The dashed line is the input pulse profile. The inset shows the transmitted pulse in linear scale, the gray region is the input pulse. (b) Calculated diffusion constant for various filling fractions. The continuous line is a best-fit by an inverse power law. The inset shows the dynamical diffusivity for two values of the particle diameters.

P_{in}. In Fig. 3(a), we show the local intensity for two input peak powers; the onset of a nonexponential tail is evident, as also shown in the inset reporting the intensity autocorrelation function. In panel (b) we show the transmitted intensity (integrated Poynting vector) for various input powers. The inset shows the instantaneous diffusivity that drops at high powers and long times, when a threshold value for the input peak power is reached. These results foster the interpretation of the data in terms of a light-induced localization transition, strongly resembling that controlled, e.g., by the packing fraction and experimentally observed (as, e.g., in Ref. [1]). However, in the present case, the transition is controlled by the input power, and hence it has a nonlinear origin. It will be shown below that it can be explained as the excitation of a "modulational instability random laser" (or random OPO).

V. THE MODULATIONAL INSTABILITY RANDOM LASER

Indeed, to unveil the underlying mechanism, we resorted to the spectral analysis of the electric field in various points inside the random medium; Fig. 4 summarizes the typical result. In panel (a) we show the calculated frequency spectra of the electric field E_y in the random structure, for different input peak powers. The data are displayed in logarithmic scale and vertically shifted by an arbitrary amount for the sake of clearness. At low power the spectrum of the input pulse is reproduced, with the addition of small ripples [due to the vertical scale in Fig. 4(a)] in correspondence of the existing high-Q modes. As the power increases, the bandwidth gets larger and regions with depression and enhancement of the spectrum appear. At sufficiently high power, a wide band excitation is found. This behavior can be explained by recalling that in $\chi^{(3)}$ media energy can be transferred from various harmonics to others through parametric amplification. We stress that the nonlinear effects are weakly perturbative, indeed we consider power level just above the OPO threshold and the nonlinear index perturbation, due to the Kerr effect, is of the order of 0.001. Thus the localization process in Fig. 3 is explained by assuming that energy is nonlinearly transferred to localized, long-living states.

In panel (b) we show the time evolution of the spectrum (i.e., the spectrogram calculated by Fourier transforming windowed parts of the temporal signal) at $P_{\text{in}}=3$ kW. In the initial interval $t<1$ ps, energy is transferred to a wide band around the input pulse spectrum. However, at large times only the long-lifetime (high Q factor) modes survive and the spectrum is characterized by several peaks in the region around $\lambda \cong 300$ nm ($\nu \cong 0.9\times 10^{15}$ Hz). In order to sustain the fact that localized modes put into oscillation, we show in the inset of Fig. 4(c) a snapshot of the electric field E_y in the sample, taken at $P=2.5$ kW and $t\cong 4$ ps which clearly show the occurrence of localized excitations with dimensions comparable to the scatterers, and corresponding the Mie resonances discussed below. Note also that these are localizations in presence of a broadband nonlinear excitation and hence many of them are present at the same instant, their different lifetimes provide the deviation from the exponential behavior of the transmitted pulse.

In addition, we repeated the pulse transmission experiment at low power $P=1$ nW and central wavelength $\lambda=300$ nm ($\sigma=400$ nm) and Fig. 4(c) clearly shows a nonexponential tail at $t\cong 2.5$ ps, which is not present for $\lambda=521$ nm [Fig. 2(a)] also for $t>3$ ps (not shown).

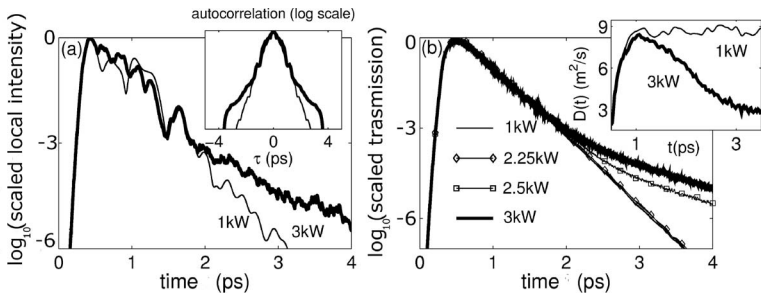

FIG. 3. (a) Time dynamics of the scaled local intensity for two different input peak powers (the peak intensity is scaled to unity); the inset shows the corresponding autocorrelation functions versus the delay τ; (b) transmitted (the peak transmission is scaled to unity) signal for various input peak powers; the inset shows the calculated instantaneous diffusivity.

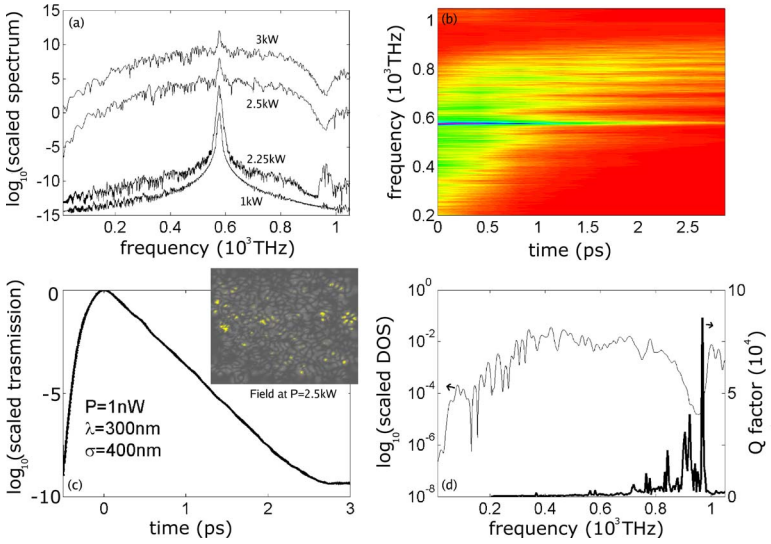

FIG. 4. (Color online) (a) Spectral emission for increasing peak power; (b) spectrogram displaying the time evolution of the spectra for $P=3$ kW; (c) normalized transmission (the peak transmission is scaled to unity) of a low power pulse at $\lambda=300$ nm and $\sigma=400$ nm displaying a nonexponential tail; the inset shows the field distribution for $\sigma=400$ nm at high power ($P=2.5$ kW) at $t=4$ ps in the xz middle section of the sample; (d) density of states (in arbitrary units) and Q-factor distribution for $\sigma=400$ nm.

Note that the deviation from the exponential trend is delayed with respect to the nonlinear regime [Fig. 3(b)], because in that case the transfer of energy to the localized modes happens in proximity of the peak of the input pulse [see also the spectrogram in Fig. 4(c)] and is more efficient so that the localized modes are much more energetic than in the case of Fig. 4(c) (where their excitation is evident only after the whole pulse has passed). In other words, as one can also see from the coupled mode theory equations addressed below, in the linear regime the energy transfer to localized modes is quadratic with time (for a constant pump beam) and weighted by an spatial overlap coefficient which is in general random and smaller with respect to delocalized modes; conversely in the nonlinear regime the energy transfer is exponential in time and is mediated by the excitation of a delocalized pump mode directly from the input pulse (see the treatment below); in addition the deviation from the exponential function in the transmission is more pronounced at higher fluences.

To discuss the origin of the localized modes we are considering, we recall that light localization is typically expected in proximity of depressions of the density of states (DOS). For the case of weakly disordered periodical structures, these are obtained inside the photonic band gaps [29], while, for random dispersions of particles, the DOS (which is numerically calculated by shining the sample by an ultrawide band single-cycle pulse and spectrally analyzing the transmitted pulse) displays some depressions (pseudogaps) in proximity of the Mie resonances (see, e.g., Refs. [8,30]). In our case, the distribution of states displays various depressions with the most pronounced around 0.9×10^{15} Hz, as shown in Fig. 4(d). The fact that localized modes do exist in proximity of the pseudogaps, is also confirmed by the plot of the calculated Q factor vs frequency [bold line in Fig. 4(d)], realized by using an harmonic inversion library [31]. Which of the localized modes are effectively excited will depend not only on the Q factors, but also on the spatial overlaps with the pump modes and with the spatial distribution of the nonlinear susceptibility. The localized modes are a reminiscence of the Mie resonances of the isolated spheres, which are strongly affected by the presence of adjacent resonators in a disordered configuration, in analogy to periodical monodispersed photonic crystal, investigated, e.g., in Ref. [32]. Thus the nonlinearly excited modes are not Anderson localization, which are sensible to the spatial extension of sample, but are due to Mie resonances, and their wavelength is shorter than the input pump wavelength.

VI. COUPLED-MODE-THEORY OF THE RANDOM OPO

Before concluding we show that the basic features of the reported results can be reproduced by a simple theoretical model, based on the coupled mode theory in the time domain (CMT) (see, e.g., Ref. [19], and references therein). Indeed the small-signal parametric gain for the four-waves interaction $\omega_0+\omega_0=(\omega_0+\Omega)+(\omega_0-\Omega)$, can be determined by introducing the complex amplitudes for the pump mode $a_0(t)=a(\omega_0,t)$ (which is directly excited by the input pump pulse) and for the generated modes $a_\pm(t)=a(\omega_0\pm\Omega,t)$. The complex amplitudes are normalized in a way such that $|a(\omega,t)|^2$ is the energy stored in the mode at angular frequency ω, and we denote with $\tau(\omega)$ the lifetime, and $Q(\omega)=\omega\tau(\omega)/2$ the corresponding Q factor. In the undepleted pump approximation the relevant CMT equations are written in compact and obvious notation as

$$\frac{da_\pm}{dt}=-\frac{1}{\tau_\pm}a_\pm+iga_0^2a_\mp^*. \tag{2}$$

The coefficient g is the relevant 3D spatial overlap between the mode electric field distributions and the nonlinear third-order susceptibility. Looking for solutions in the form $a_\pm=A_\pm\exp(\alpha t)$, the real-valued gain α is given by

$$\alpha=-\left(\frac{1}{2\tau_+}+\frac{1}{2\tau_-}\right)+\left[\left(\frac{1}{2\tau_+}-\frac{1}{2\tau_-}\right)^2+|ga_0^2|^2\right]^{1/2}. \tag{3}$$

It is readily seen that a condition for having amplification ($\alpha>0$) is given by $|ga_0^2|^2>1/(\tau_+\tau_-)=\omega_+\omega_+/4Q_+Q_-$. Assuming that for all the involved modes $\omega\cong\omega_0$ and the Q factor is almost the same, with the exception of those localized that display higher values, it is concluded that the localized

modes (those with not negligible overlap g with the pump modes) are put into oscillations at lower pump energies [see line at 2.25 kW in Fig. 4(a)]. Additionally the asymmetry, at low power, in the spectrum [see Fig. 4(a)] can be explained by observing from Eq. (2) that $|A_+/A_-|>1$ if $Q_+>Q_-$. At higher powers most of the modes are put into oscillation and the spectrum mimics the DOS.

VII. CONCLUSION

In conclusion, the considered disordered, nonlinear and dispersive samples support localized modes in proximity of Mie resonances. These can be excited by high-intensity pulses through optical parametric amplification. The overall process can be interpreted as the excitation of a "modulational instability random laser." The main difference with standard random lasers is given by the fact that an ultrafast optical process provides the required gain and does not need doping of the sample by an active media. These results can be generalized to other nonlinear amplification processes, such as the Raman effect, and can find application in all-optical storage of light, ultrafast laser-tissue interaction, soft-matter and granular systems.

ACKNOWLEDGMENTS

We thank S. Trillo and D. Wiersma for fruitful discussions. We acknowledge support from the INFM-CINECA initiative for parallel computing.

[1] M. Storzer, P. Gross, C. M. Aegerter, and G. Maret, Phys. Rev. Lett. **96**, 063904 (2006).
[2] A. A. Chabanov, B. Hu, and A. Z. Genack, Phys. Rev. Lett. **93**, 123901 (2004).
[3] P. M. Johnson, A. Imhof, B. P. J. Bret, J. G. Rivas, and A. Lagendijk, Phys. Rev. E **68**, 016604 (2003).
[4] D. S. Wiersma, P. Bartolini, A. Lagendijk, and R. Righini, Nature (London) **390**, 671 (1997).
[5] F. Reil and J. E. Thomas, Phys. Rev. Lett. **95**, 143903 (2005).
[6] M. C. W. van Rossum and T. M. Nieuwenhuizen, Rev. Mod. Phys. **71**, 313 (1999).
[7] S. E. Skipetrov and B. A. van Tiggelen, Phys. Rev. Lett. **96**, 043902 (2006).
[8] C. Vanneste and P. Sebbah, Phys. Rev. E **71**, 026612 (2005).
[9] S. K. Cheung and Z. Q. Zhang, Phys. Rev. B **72**, 235102 (2005).
[10] P. Markos and C. M. Soukoulis, Phys. Rev. B **71**, 054201 (2005).
[11] S. H. Tseng, A. Taflove, D. Maitland, V. Backman, and J. T. Walsh, Jr., Opt. Express **13**, 6127 (2005).
[12] H. Cao, J. Phys. A **38**, 10497 (2005).
[13] S. Mujumdar, M. Ricci, R. Torre, and D. S. Wiersma, Phys. Rev. Lett. **93**, 053903 (2004).
[14] B. Liu, A. Yamilov, Y. Ling, J. Y. Xu, and H. Cao, Phys. Rev. Lett. **91**, 063903 (2003).
[15] L. I. Deych, Phys. Rev. Lett. **95**, 043902 (2005).
[16] L. Angelani, C. Conti, G. Ruocco, and F. Zamponi, Phys. Rev. Lett. **96**, 065702 (2006); Phys. Rev. B **74**, 104207 (2006).
[17] B. Spivak and A. Zyuzin, Phys. Rev. Lett. **84**, 1970 (2000).
[18] S. E. Skipetrov, Phys. Rev. E **67**, 016601 (2003).
[19] C. Conti, A. Di Falco, and G. Assanto, Opt. Express **12**, 823 (2004).
[20] M. A. Foster, A. C. Turner, J. E. Sharping, B. S. Schmidt, M. Lipson, and A. L. Gaeta, Nature (London) **441**, 960 (2006).
[21] T. J. Kippenberg, S. M. Spillane, and K. J. Vahala, Phys. Rev. Lett. **93**, 083904 (2004).
[22] M. Nakazawa, K. Suzuki, and H. A. Haus, IEEE J. Quantum Electron. **25**, 2036 (1989).
[23] L. Angelani, G. Foffi, F. Sciortino, and P. Tartaglia, J. Phys.: Condens. Matter **17**, L113 (2005); we used the data at temperature $T=0.26$ in the units of this reference.
[24] I. M. Vellekoop, P. Lodahl, and A. Lagendijk, Phys. Rev. E **71**, 056604 (2005).
[25] J. R. DeVore, J. Opt. Soc. Am. **41**, 416 (1951).
[26] A. Taflove and S. C. Hagness, *Computational Electrodynamics: The Finite-difference Time-Domain Method*, 3rd ed. (Artech House, Boston, 2000).
[27] C. Conti, A. Di Falco, and G. Assanto, Opt. Lett. **29**, 2902 (2004).
[28] A. A. Chabanov, Z. Q. Zhang, and A. Z. Genack, Phys. Rev. Lett. **90**, 203903 (2003).
[29] S. John, Phys. Rev. Lett. **58**, 2486 (1987).
[30] A. A. Chabanov and A. Z. Genack, Phys. Rev. Lett. **87**, 153901 (2001).
[31] V. A. Mandelshtam, Prog. Nucl. Magn. Reson. Spectrosc. **38**, 159 (2001); we used the Harminv library by Steven G. Johnson (MIT).
[32] C. Vandenbem and J. P. Vigneron, J. Opt. Soc. Am. A **22**, 1042 (2005).